Eur. Phys. J. E **23**, 135–144 (2007)
DOI 10.1140/epje/i2007-10188-1

THE EUROPEAN PHYSICAL JOURNAL E

Finite-stretching corrections to the Milner-Witten-Cates theory for polymer brushes

J.U. Kim[a] and M.W. Matsen[b]

Department of Mathematics, University of Reading, Whiteknights, Reading RG6 6AX, UK

Received 6 March 2007 and Received in final form 24 April 2007
Published online: 6 June 2007 –

Abstract. This paper investigates finite-stretching corrections to the classical Milner-Witten-Cates theory for semi-dilute polymer brushes in a good solvent. The dominant correction to the free energy originates from an entropic repulsion caused by the impenetrability of the grafting surface, which produces a depletion of segments extending a distance $\mu \propto L^{-1}$ from the substrate, where L is the classical brush height. The next most important correction is associated with the translational entropy of the chain ends, which creates the well-known tail where a small population of chains extend beyond the classical brush height by a distance $\xi \propto L^{-1/3}$. The validity of these corrections is confirmed by quantitative comparison with numerical self-consistent field theory.

PACS. 68.47.Pe Langmuir-Blodgett films on solids; polymers on surfaces; biological molecules on surfaces – 61.41.+e Polymers, elastomers, and plastics

1 Introduction

A simple and effective method of modifying surface properties is to graft polymer chains to the surface by one of their ends producing a so-called brush [1]. The presence of the brush can, for example, reduce surface friction, prevent corrosion of the substrate, improve biocompatibility, modify adhesion, alter wetting properties, and create a steric repulsion combating van der Waals attractions. This paper focuses on brushes with high grafting densities and long flexible chains. Furthermore, it assumes they are immersed in a good solvent that dilutes the polymer, forcing the chains to stretch away from the grafting surface.

The above assumptions permit a simple theoretical treatment. When the chains are long and flexible, they can be modeled as thin elastic threads commonly referred to as Gaussian chains [2]. A high grafting density implies a significant overlap between the chains, allowing the molecular interactions to be represented by a mean field, $w(z)$, where z is the distance from the substrate. Provided the brush is not too concentrated, $w(z)$ is simply proportional to the average polymer concentration, $\phi(z)$. The concentration is evaluated from the propagator, $q(z, z_0, s)$, which represents the partition function for a fraction, s, of a chain in the field $w(z)$ with its ends constrained at z and z_0. For Gaussian chains, $q(z, z_0, s)$ satisfies a modified diffusion equation. Although this self-consistent field theory (SCFT) [2] is relatively simple, it still needs to be solved numerically.

There is one useful limit where an analytical approximation becomes possible. As Milner *et al.* [3] have pointed out, the diffusion equation for $q(z, z_0, s)$ is analogous to the Schrödinger wave equation for a single particle in the inverted well, $-w(z)$, where s plays the role of time. When the chains become strongly stretched, the quantum-mechanical analogy reduces to that of a classical mechanical problem. The fact that all chains in the brush must reach the substrate in a fixed unit of time (*i.e.*, from $s = 0$ to 1) implies that the potential must be that of a harmonic oscillator, for which the analytical solution is known. (Semenov [4] actually had arrived at the same conclusion a few years earlier by another means.) The two principle successes of this strong-stretching theory (SST) are the predictions that $\phi(z)$ is parabolic and that the chain ends are distributed throughout the brush; prior to that, researchers used the Alexander ansatz [5], which assumed a uniform profile with all the chain ends located at the outer edge of the brush. Still the SST misses a couple of key features, such as a depletion of segments next to the substrate. It also predicts an absolute thickness, L, beyond which $\phi(z) = 0$, whereas in reality there is a tail over which $\phi(z)$ gradually decays. The more complete SCFT [6–8] captures these extra features and indeed shows good agreement with both experiment [6,9] and simulation [10–12]. Unfortunately though, the numerical SCFT does not provide the same degree of insight as

[a] e-mail: j.kim@reading.ac.uk
[b] e-mail: m.w.matsen@reading.ac.uk

the analytical SST, and thus there is considerable value to be gained by improving upon the SST approach.

There have been a number of papers investigating corrections to SST. For instance, the tail has been examined by two different analytical calculations [13,14] and one numerical treatment [15]. These studies found that the characteristic length of the tail scales as $\xi \sim L^{-1/3}$, and they provided predictions for $\phi(z)$ in the extremity of the tail ($z \gtrsim L + \xi$), although there are slight ambiguities among the different approaches. The depletion layer, on the other hand, has received almost no theoretical attention apart from an old calculation by de Gennes [16] based on the Alexander approach [5]. He predicted that the width of the depletion layer scales as the spacing between grafting points and suggested a shape for $\phi(z)$ within the layer.

Here we develop a more sophisticated treatment of the depletion layer by adapting a theory introduced by Likhtman and Semenov [17] for dry brushes. It predicts a universal shape for $\phi(z)$ with a characteristic width that scales as $\mu \sim L^{-1}$, which we confirm with quantitative comparisons to SCFT. We also use SCFT to examine the tail region in much greater detail to previous studies. This reveals a universal shape for the entire tail ($z > L$), which at sufficiently large z converges to an analytical prediction obtained using the approach of Witten and Milner [13]. We conclude our study by deriving an accurate expression for the free energy of the brush.

2 Theory

Before describing our various theoretical methods, we outline the details of the underlying model for a brush with n polymer chains grafted to a flat substrate of area, $\mathcal{A}$, at $z = 0$. Each polymer occupies a fixed volume of N/ρ_0 and has a natural end-to-end length of $aN^{1/2}$, where N is the degree of polymerization, ρ_0 represents the segment density in a pure melt, and a is the statistical segment length. The configuration of the α-th chain is specified by the space curve, $\mathbf{r}_\alpha(s)$, where s is a parameter that runs along the polymer backbone increasing from 0 at the free end to 1 at the grafted end. With that, we can then define the dimensionless polymer concentration,

$$\hat{\phi}(\mathbf{r}) = \frac{N}{\rho_0} \sum_{\alpha=1}^{n} \int_0^1 \delta(\mathbf{r} - \mathbf{r}_\alpha(s)) \mathrm{d}s \,. \tag{1}$$

The remaining space is then filled with solvent molecules, each of volume v_s, producing a uniform concentration of one in dimensionless units. The solvent degrees of freedom can be integrated out, producing the effective Hamiltonian,

$$\frac{H[\{\mathbf{r}_\alpha\}]}{k_B T} = \frac{3}{2a^2 N} \sum_{\alpha=1}^{n} \int_0^1 |\mathbf{r}'_\alpha(s)|^2 \mathrm{d}s + \frac{v\rho_0}{2} \int \hat{\phi}^2(\mathbf{r}) \mathrm{d}\mathbf{r} \,, \tag{2}$$

where the first integral represents the entropic penalty of stretching polymer chains and the second integral involves the excluded-volume parameter, $v \equiv (v_s\rho_0)^{-1} - 2\chi$. The first term of v accounts for the translational entropy of the solvent assuming its concentration is relatively high [18], and the second term involves the Flory-Huggins polymer-solvent interaction parameter, χ. (Note that it is common practice to define the polymer segment volume equal to that of the solvent, in which case $v_s\rho_0 = 1$.)

Provided that the polymer brush is not too dilute, the segment interactions can be represented by a mean field,

$$w(z) = vN \left\langle \hat{\phi}(\mathbf{r}) \right\rangle \,, \tag{3}$$

where the angle brackets denote an ensemble average. By symmetry, the field is uniform in the x and y directions and thus $x_\alpha(s)$ and $y_\alpha(s)$ obey random-walk statistics, while $z_\alpha(s)$ obeys Boltzmann statistics with an energy, $E[z_\alpha; 1]$, defined by

$$\frac{E[z_\alpha; s]}{k_B T} = \int_0^s \left[\frac{3}{2a^2 N} |z'_\alpha(t)|^2 + w(z_\alpha(t)) \right] \mathrm{d}t \,. \tag{4}$$

For convenience, the grafting density, $\sigma \equiv n/\mathcal{A}$, can be removed from the problem by defining the scaled concentration,

$$\phi(z) = \frac{a\rho_0}{\sigma N^{1/2}} \left\langle \hat{\phi}(\mathbf{r}) \right\rangle \,, \tag{5}$$

normalized such that

$$\int_0^\infty \phi(z) \mathrm{d}z = aN^{1/2} \,. \tag{6}$$

The field equation is then rewritten as

$$w(z) = \Lambda \phi(z) \,, \tag{7}$$

where the reduced interaction parameter is defined as

$$\Lambda \equiv \frac{v\sigma N^{3/2}}{a\rho_0} \,. \tag{8}$$

Likewise, the degree of polymerization, N, can be scaled out of the problem by simply expressing all lengths in terms of $aN^{1/2}$. Thus the brush can be characterized by the single parameter, Λ, and therefore there is no need for us to explicitly discuss how the various quantities vary with respect to σ or N; it is sufficient to know how they vary with Λ or alternatively L (see Eq. (25)).

2.1 Self-consistent field theory (SCFT)

We now describe the exact mean-field treatment generally referred to as self-consistent field theory (SCFT) [6–8]. Underpinning the calculations is the partition function,

$$q(z, z_0, s) \propto \int \mathcal{D}z_\alpha \exp\left(-\frac{E[z_\alpha; s]}{k_B T} \right) \times \delta(z_\alpha(0) - z_0) \delta(z_\alpha(s) - z) \,, \tag{9}$$

for a fragment of sN segments with its ends fixed at $z_\alpha(0) = z_0$ and $z_\alpha(s) = z$. It is evaluated by solving the modified diffusion equation [2,19],

$$\frac{\partial}{\partial s} q(z, z_0, s) = \left[\frac{a^2 N}{6} \frac{\partial^2}{\partial z^2} - w(z) \right] q(z, z_0, s) \,, \tag{10}$$

subject to the initial condition, $q(z, z_0, 0) = \delta(z - z_0)aN^{1/2}$, and the boundary condition, $q(0, z_0, s) = 0$.

Once $q(z, z_0, s)$ is determined, the concentration profile for a single chain with its free end at $z = z_0$ is given by

$$\phi(z; z_0) = \int_0^1 \frac{q(\epsilon, z, 1-s)q(z, z_0, s)}{q(\epsilon, z_0, 1)} \mathrm{d}s \,. \tag{11}$$

(Note that numerical calculations must be done with the grafting point at a small distance, ϵ, from the substrate.) The probability that the free end ($s = 0$) occurs at z_0 is given by

$$g(z_0) = \frac{aN^{1/2}q(\epsilon, z_0, 1)}{\int_0^\infty q(\epsilon, z, 1)\mathrm{d}z} \,, \tag{12}$$

which allows us to evaluate the overall segment concentration using

$$\phi(z) = \frac{1}{aN^{1/2}} \int_0^\infty g(z_0)\phi(z; z_0)\mathrm{d}z_0 \,. \tag{13}$$

As usual, the field has to be adjusted such that the concentration satisfies the field equation (7). This is done by a numerical method analogous to that used in reference [20] for dry brushes.

After the field has been determined self-consistently, the free energy of the brush can be evaluated as

$$\frac{F}{nk_BT} = \frac{1}{aN^{1/2}} \int_0^\infty g(z_0) \left[\frac{f_e(z_0)}{k_BT} + \ln g(z_0) \right] \mathrm{d}z_0 + \frac{\Lambda}{2aN^{1/2}} \int_0^\infty \phi^2(z)\mathrm{d}z \,. \tag{14}$$

The first term is an average of

$$\frac{f_e(z_0)}{k_BT} = -\ln q(\epsilon, z_0, 1) - \frac{1}{aN^{1/2}} \int_0^\infty w(z)\phi(z; z_0)\mathrm{d}z \,, \tag{15}$$

which represents the stretching energy of extending a chain to z_0. The second term, involving $g(z_0)\ln g(z_0)$, accounts for the translational entropy of the free ends, and the last term is the average interaction energy.

2.2 Full classical theory (FCT)

If the polymer chains are highly stretched, we can implement a useful approximation [7,21,22] by assuming that each polymer is restricted to the trajectory, $z_\alpha(s)$, that minimizes $E[z_\alpha; 1]$, in which case the partition function becomes

$$q(0, z_0, 1) \propto \exp(-E[z_\alpha; 1]/k_BT) \,. \tag{16}$$

This is called the full classical theory (FCT), because the lowest-energy trajectories are obtained by appealing to an analogy with a completely distinct problem involving the classical mechanics of a particle sliding down an incline [19]. By interpreting s as time, $3/a^2N$ as mass, and $z_\alpha(s)$ as the position of the particle, the quantity $E[z_\alpha; 1]$ then corresponds to the action of the particle in the inverted potential, $-w(z)$. Thus the problem of determining the polymer path of lowest energy is equivalent to the classical mechanics problem, where a particle starts at $z_\alpha(0) = z_0$ and finishes at $z_\alpha(1) = 0$. (In the absence of chain fluctuations, we can now set $\epsilon = 0$.)

Using classical mechanics, the dimensionless speed at position z is

$$S(z; z_0) \equiv \frac{|z'|}{aN^{1/2}} = \left(v^2(z_0) - \frac{2}{3}[w(z_0) - w(z)] \right)^{1/2} \,, \tag{17}$$

where $v(z_0)$ is the initial velocity at $z = z_0$. For weakly stretched chains, $v(z_0) > 0$ in which case the trajectory first extends outward to $z = z_m$ as determined by $S(z_m; z_0) = 0$, before it reverses direction back towards the substrate. For strongly stretched chains, the trajectory approaches the substrate monotonically and thus $z_m = z_0$. Note that the division between these two behaviors coincides with the peak in $g(z_0)$ [7].

The concentration of segments along the polymer path is given by $N|\mathrm{d}s/\mathrm{d}z|$, which is inversely proportional to the speed of our imaginary particle. Thus the segment distribution for a chain starting from z_0 is given by

$$\phi(z; z_0) = \begin{cases} 1/S(z; z_0) \,, & \text{if } 0 < z < z_0 \,, \\ 2/S(z; z_0) \,, & \text{if } z_0 < z < z_m \,, \\ 0 \,, & \text{if } z_m < z \,. \end{cases} \tag{18}$$

The factor of 2, for $z_0 < z < z_m$, follows from the fact that the trajectory transverses the interval in both directions. By noting that the total number of segments in a chain is N, we obtain the constraint,

$$\frac{1}{aN^{1/2}} \int_0^\infty \phi(z; z_0)\mathrm{d}z = 1 \,, \tag{19}$$

which is used to determine $v(z_0)$. Once the trajectories are known, $E[z_\alpha; 1]$ is evaluated with equation (4), $q(0, z_0, 1)$ is then determined by equation (16), $g(z_0)$ follows from equation (12), and $\phi(z)$ is obtained with equations (13) and (18). As with SCFT, $w(z)$ must be adjusted so as to satisfy equation (7), after which the free energy can be evaluated using equation (14). Despite the extra approximations, this still remains a numerical calculation.

2.3 Strong-stretching theory (SST)

To obtain the analytical strong-stretching theory (SST) of Milner *et al.* [3], one must assume that the chains are so stretched that the tension at their free ends is relatively negligible, which implies $v(z_0) \approx 0$. In terms of the classical mechanical analogy, the trajectories, $z_\alpha(s)$, must then start from rest and arrive at the substrate in one unit of time regardless of their starting points. The only potential that satisfies this is

$$w_0(z) = \frac{3\pi^2(L^2 - z^2)}{8a^2N} \,, \tag{20}$$

for which the trajectory is

$$z_\alpha(s) = z_0 \cos(\pi s/2)\,. \tag{21}$$

Notice that the classical potential in equation (20) involves a constant, L, which will ultimately be interpreted as an absolute brush thickness, beyond which the field and thus the segment concentration are identically zero.

For these simple harmonic trajectories, the segment concentration in equation (18) reduces to

$$\phi_0(z;z_0) = \begin{cases} \frac{2aN^{1/2}}{\pi\sqrt{z_0^2-z^2}}\,, & \text{if } z < z_0\,, \\ 0\,, & \text{if } z > z_0\,. \end{cases} \tag{22}$$

At this level of approximation, all trajectories have the same energy,

$$\frac{E[z_\alpha;1]}{k_BT} = \frac{3\pi^2L^2}{8a^2N}\,, \tag{23}$$

regardless of their starting point, which implies that $g_0(z_0)$ is a constant. This is because the SST approximation is too crude for the use of equation (12), but fortunately we can calculate $\phi_0(z)$ without $g_0(z_0)$ since we already know the field. (Note that SST quantities are denoted with a subscript of 0.) From equations (6) and (7), it immediately follows that

$$\phi_0(z) = \frac{3(L^2-z^2)aN^{1/2}}{2L^3}\,, \tag{24}$$

where the classical brush height is given by

$$\frac{L}{aN^{1/2}} = \left(\frac{4\Lambda}{\pi^2}\right)^{1/3} = \left(\frac{4v\sigma}{\pi^2 a\rho_0}\right)^{1/3} N^{1/2}\,. \tag{25}$$

(Note that this relation allows us to characterize the brush with the quantity, $L/aN^{1/2}$, instead of Λ.) Now that $\phi(z)$ is known, we can use equation (13) to evaluate the end-segment distribution as

$$g_0(z_0) = \frac{3z_0aN^{1/2}}{L^3}\sqrt{L^2-z_0^2}\,. \tag{26}$$

Substituting the above results into equation (14), the classical free energy works out to be

$$\frac{F_0}{nk_BT} = \frac{9\pi^2}{40}\left(\frac{L}{aN^{1/2}}\right)^2 - \frac{5}{3} + \ln\left(\frac{6aN^{1/2}}{L}\right)\,. \tag{27}$$

The constant and logarithmic terms, which originate from the translational entropy of the end-segment distribution, are usually neglected because they are small relative to the L^2 term. In the interest of developing an improved approximation to SCFT, these terms are now retained. Furthermore, $\ln(2/\sqrt{3})$ must be added to equation (27) to account for the unspecified proportionality factor in equation (9). The need for this extra constant is easily demonstrated by examining a chain in the harmonic potential. In SST, the free energy is given by equation (23), but in SCFT, the free energy is

$$-\ln q(0,z_0,1) = \frac{3\pi^2L^2}{8a^2N} + \ln\left(\frac{2}{\sqrt{3}}\right)\,, \tag{28}$$

where

$$q(z,z_0,s) = \left(\frac{3}{4\sin(\pi s/2)}\right)^{1/2} \exp\left(-\frac{3\pi^2L^2s}{8a^2N} - \frac{3\pi[(z^2+z_0^2)\cos(\pi s/2) - 2zz_0]}{4a^2N\sin(\pi s/2)}\right) \tag{29}$$

is the appropriate solution of the diffusion equation (10). (Note that this solution does not enforce the $q(0,z_0,s)=0$ boundary condition, because that will be accounted for in the next section.)

2.4 Depletion layer

In this section, we develop a new calculation for the depletion layer, which follows a previous theory of Likhtman and Semenov [17] for dry brushes. There the grafting surface was treated as a reflecting boundary [19] and could be ignored until the very end, at which point the segment concentration at negative z was just reflected to positive z. Here we must invoke the zero boundary condition from the very start. Otherwise, the details of the calculation [23] remain much the same, which allow us to skip a few parts of the derivation.

The calculation starts by considering a single chain with its $s=0$ end at $z=z_0$ and its $s=1$ end slightly removed from the substrate at $z=\epsilon$. In the region near the substrate, the chain tension, τk_BT, is given by

$$\tau \equiv \frac{3}{a^2N}z'_\alpha(1) = \frac{3\pi z_0}{2a^2N}\,. \tag{30}$$

This observation allows us to approximate the concentration next to the substrate by

$$\phi(z;z_0) \approx \frac{\int_0^1 \mathrm{d}s \int_0^\infty \mathrm{d}z_1 q(\epsilon,z,1-s)q(z,z_1,s)\exp(\tau z_1)}{\int_0^\infty q(\epsilon,z_1,1)\exp(\tau z_1)\mathrm{d}z_1}\,, \tag{31}$$

where the parabolic potential is removed and replaced by the appropriate external tension. Following the same steps described in reference [23] for dry brushes, we arrive at the approximation,

$$\phi(z;z_0) \approx \psi_1(z)\psi_2(z)\,, \tag{32}$$

where

$$\psi_1(z) \equiv \frac{aN^{1/2}}{\epsilon}\int_0^\infty q(\epsilon,z,s)\exp\left(-\frac{a^2N}{6}\tau^2 s\right)\mathrm{d}s\,, \tag{33}$$

$$\psi_2(z) \equiv \frac{\epsilon}{aN^{1/2}}\frac{\int_0^\infty q(z,z_1,1)\exp(\tau z_1)\mathrm{d}z_1}{\int_0^\infty q(\epsilon,z_1,1)\exp(\tau z_1)\mathrm{d}z_1}\,. \tag{34}$$

In this current derivation, factors of ϵ must be inserted so that $\psi_1(z)$ and $\psi_2(z)$ remain finite in the limit $\epsilon \to 0$. Although $\psi_1(z)$ has no simple physical interpretation, $\psi_2(z)$ involves the ratio of two partition functions for chains with one end under the external tension, τk_BT, and the other end fixed at either z or ϵ.

It follows from equation (10) that $\psi_2(z)$ satisfies

$$\frac{a^2N}{6}\frac{\partial^2}{\partial z^2}\psi_i(z) = \left(\frac{a^2N}{6}\tau^2 + \Delta w(z)\right)\psi_i(z)\,, \qquad (35)$$

where

$$\Delta w(z) \equiv w(z) - w_0(0)\,, \qquad (36)$$

$$= \Lambda\phi(z) - \frac{3\pi^2L^2}{8a^2N}\,. \qquad (37)$$

The definition in equation (34) also implies that $\psi_2(0) = 0$ and $\psi_2(\epsilon) = \epsilon/aN^{1/2}$. By taking the limit $\epsilon \to 0$, the latter condition reduces to $\psi_2'(0) = 1/aN^{1/2}$. Similarly, $\psi_1(z)$ also satisfies equation (35) but with a delta function, $\delta(z-\epsilon)a^2N/\epsilon$, subtracted from the right-hand side, and its definition in equation (33) implies the boundary conditions, $\psi_1(0) = \psi_1(\infty) = 0$. The only effect of the delta function is to cause a rapid rise from $\psi_1(0) = 0$ to $\psi_1(\epsilon) = 6$. Thus in the limit of $\epsilon \to 0$, we can disregard the delta function and just use equation (35), provided we set $\psi_1(0) = 6$ rather than zero.

Once the $\psi_i(z)$ are solved for the full range of tensions (or equivalently, z_0 values), the overall concentration is given by

$$\phi(z) = \int_0^L g_0(z_0)\psi_1(z)\psi_2(z)\mathrm{d}z_0\,. \qquad (38)$$

Naturally $\Delta w(z)$ must be adjusted so that $\phi(z)$ satisfies the self-consistent condition in equation (37). After that, the entropic energy loss due the substrate is calculated for each chain using

$$\frac{\Delta f_e(z_0)}{k_BT} = \ln\left[\lim_{z\to\infty}\psi_2(z)\exp(-\tau z)aN^{1/2}/\epsilon\right] - \frac{1}{aN^{1/2}}\int_0^\infty \Delta w(z)\phi(z;z_0)\mathrm{d}z\,, \qquad (39)$$

and then averaged over $g_0(z_0)$. Of course, the depletion of segments also affects the internal energy; we estimate this effect by

$$\frac{\Delta F_u}{nk_BT} = \frac{\Lambda}{aN^{1/2}}\left[\int_0^\infty \frac{\phi^2(z)-\phi_0^2(0)}{2}\mathrm{d}z + \Sigma\phi_0(0)\right], \qquad (40)$$

where

$$\Sigma \equiv \int_0^\infty [\phi_0(0) - \phi(z)]\mathrm{d}z \qquad (41)$$

represents the number of displaced segments. The integral in equation (40) provides the reduction in enthalpy caused by the removal of segments from the depletion layer, while the second term estimates the increased enthalpy of depositing them in the region beyond the depletion layer. This assumes that the vast majority of segments, Σ, are deposited not too far from the substrate, where the polymer concentration is still well approximated by $\phi_0(0)$. The justification for this will come in Section 3.1.

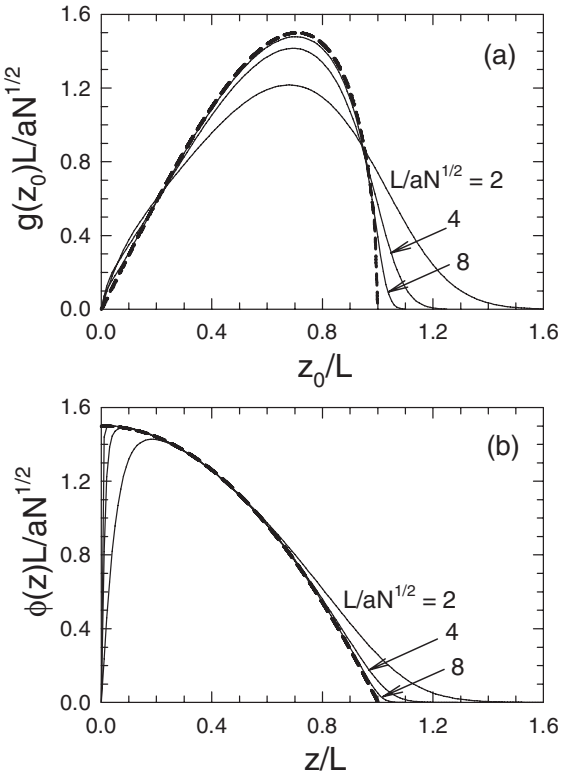

Fig. 1. (a) End-segment distributions and (b) concentration profiles. Solid curves are calculated with SCFT for various brush thicknesses, L, and dashed curves show the $L \to \infty$ limit predicted by SST.

3 Results

Our SCFT results for the end-segment distribution, $g(z_0)$, and the overall concentration, $\phi(z)$, are shown in Figures 1a and b, respectively, and are analogous to those calculated earlier by Netz and Schick [7,24]. As expected, the SCFT curves ultimately converge to the SST predictions (dashed curves) in equations (26) and (24) once the brush becomes sufficiently thick. However, for moderate thicknesses, there are two distinct regions where the SCFT profiles differ significantly from the classical parabolic shape: the depletion layer near $z \approx 0$ and the tail region near $z \approx L$. In the following sections, we examine these two regions separately and then conclude by investigating their combined effect on the free energy.

3.1 Depletion layer

This section focuses on the depletion of segments in Figure 1b next to the substrate. A crude analytical estimate of the effect can be obtained by neglecting the field (*i.e.*, setting $\Delta w(z) = 0$). In this case, $\psi_1(z) = 6\exp(-\tau z)$ and $\psi_2(z) = \sinh(\tau z)/\tau aN^{1/2}$, from which it follows that

$$\phi(z;z_0) \approx \frac{3}{\tau aN^{1/2}}(1 - \exp(-2\tau z))\,. \qquad (42)$$

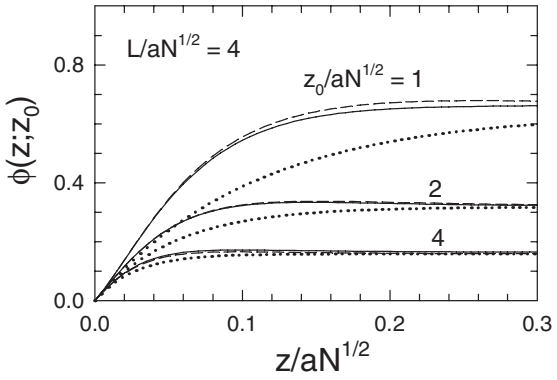

Fig. 2. Segment profiles near the substrate for individual chains with different end points, z_0, in a brush of thickness $L/aN^{1/2} = 4$. The dotted curves show the estimate from equation (42) assuming $\Delta w(z) = 0$, dashed curves show the predictions with $\Delta w(z)$ satisfying equation (37), and the solid curves are the full SCFT.

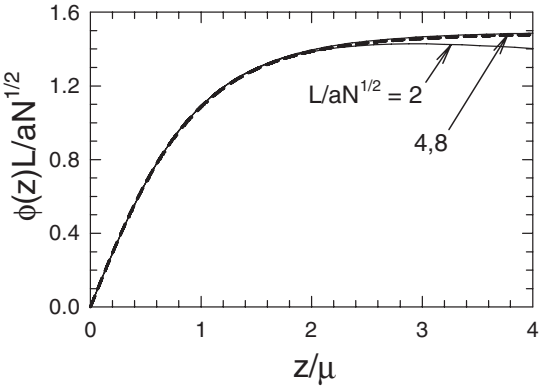

Fig. 3. Concentration profiles of the depletion layer plotted for $L/aN^{1/2} = 2$, 4 and 8, where the distance from the substrate is scaled by μ. The dashed curve denotes the scaling result predicted by equation (38).

Hence, the range over which the segment profiles are depleted is roughly $(2\tau)^{-1} = a^2N/3\pi z_0$, and the total number of displaced segments is $3/2\tau^2 aN^{1/2} \propto z_0^{-2}$. Therefore, the weakly stretched chains are by far the most affected, which provides our justification for equation (40).

Figure 2 compares the analytical profile in equation (42) with actual SCFT predictions for chains extending to $z_0/aN^{1/2} = 1$, 2, and 4 in a brush of thickness $L/aN^{1/2} = 4$. Even with this simple treatment, the agreement is reasonable, particularly when the chains are strongly stretched. However, when the field is adjusted to satisfy the self-consistent condition in equation (37), the agreement becomes nearly perfect.

It is interesting to note that all the curves in Figure 2 start off with the exact same slope regardless of z_0 or whether $\Delta w(z)$ is solved self-consistently or is simply set to zero. This is verified by inserting the initial conditions for $\psi_i(z)$ into

$$\phi'(0; z_0) = \psi_1'(0)\psi_2(0) + \psi_1(0)\psi_2'(0) = \frac{6}{aN^{1/2}}. \qquad (43)$$

Of course, if this condition applies to each individual chain, it must also apply to the total concentration, $\phi(z)$.

The overall width of the depletion layer, μ, is estimated by averaging $(2\tau)^{-1}$ over the classical end-segment distribution in equation (26), which predicts

$$\mu \equiv \frac{a^2N}{3\pi}\int_0^L \frac{g_0(z_0)}{z_0}\mathrm{d}z_0 = \frac{a^2N}{4L}. \qquad (44)$$

This dependence of the width on L can be removed by using the scaling quantities: z/μ, $\mu\tau$, $\mu^2\Delta w$, ψ_1, and ψ_2/μ. By doing so, equation (38) provides a universal shape for the concentration profile next to the substrate, shown in Figure 3 with a dashed curve. When compared to SCFT for $L/aN^{1/2} = 2$, 4 and 8, only the most weakly stretched brush shows any appreciable departure from the prediction. This is because a significant reduction in the classical parabolic profile, $\phi_0(z)$, occurs before $z \gg \mu$.

3.2 Tail region

Our attention now turns to the tail that extends beyond the classical cut-off at L. It exists for two reasons: first, the translational entropy of the chain ends causes a broadening of $g(z_0)$, and second, fluctuations about the classical trajectories cause a further spread in the concentration. It will become evident from the good agreement between FCT and SCFT that the chain fluctuations are relatively unimportant.

To investigate the shape of the tail, we extend a classical derivation developed by Milner and Witten [13]. It follows the FCT where $g(z_0) \propto \exp(-E[z_\alpha; 1]/k_BT)$, but to keep the calculation analytical, it assumes the parabolic field for $z < L$ and zero field for $z > L$. This defines a clear division, $z_\alpha(f) = L$, along the classical trajectory separating the part of the chain $(0 < s < f)$ outside the brush from the part $(f < s < 1)$ inside. The amount of chain extending beyond L is well approximated by

$$f \approx \frac{2}{\pi}\sqrt{\frac{z_0 - L}{L}}, \qquad (45)$$

provided that $f \ll 1$. Once f is determined, the complete trajectory and its energy, $E[z_\alpha; 1]$, are easily calculated giving

$$g(z_0) \approx kg(L)\exp\left(-\pi\left(\frac{z_0 - L}{\xi}\right)^{3/2}\right), \qquad (46)$$

where the length of the tail,

$$\xi \equiv L^{-1/3}a^{4/3}N^{2/3}, \qquad (47)$$

emerges naturally. Because of the approximations involved, equation (46) only applies to $z_0 \gtrsim L + \xi$, which is why the prefactor, k, must be inserted. Figure 4a confirms that the functional form agrees with our SCFT results, and estimates $k \approx 1.34$ by fitting to $L/aN^{1/2} = 8$.

Although there is no simple analytical expression for the entire tail, Figure 4b demonstrates that it, nevertheless, has a universal shape. By plotting $g(z_0)/g(L)$ *versus*

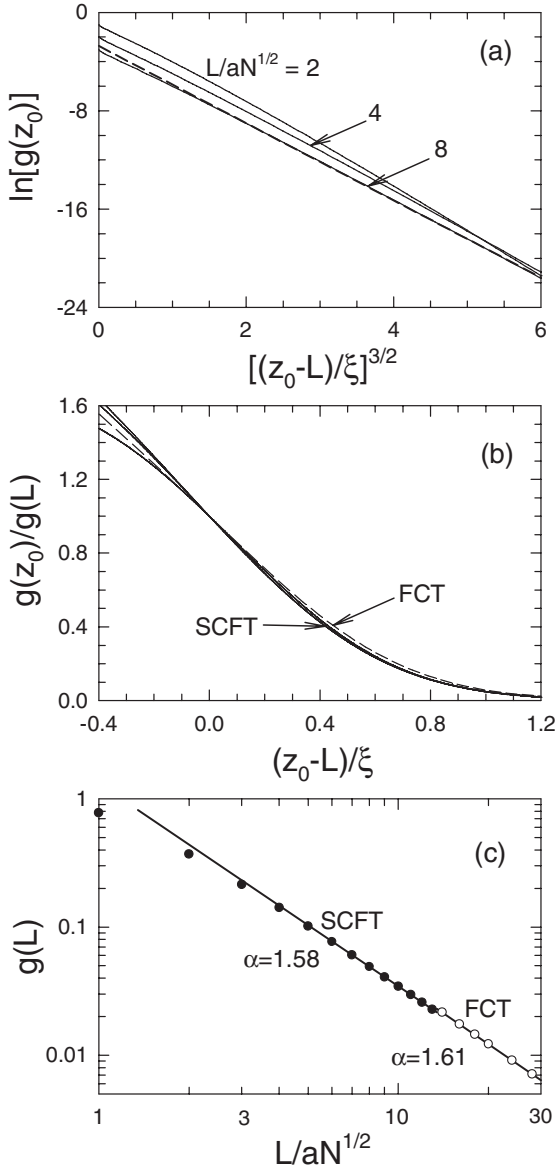

Fig. 4. (a) Tail of the end-segment distribution plotted so as to test the functional form of equation (46); the dashed line is a fit to $L/aN^{1/2} = 8$ with $k = 1.34$. (b) Scaling plot that collapses the three SCFT distributions in Figure 1a onto a single master curve; the dashed curve shows the master curve for FCT. (c) Plot demonstrating the power law behavior, $g(L) \sim L^{-\alpha}$, for SCFT (solid circles) and FCT (open circles).

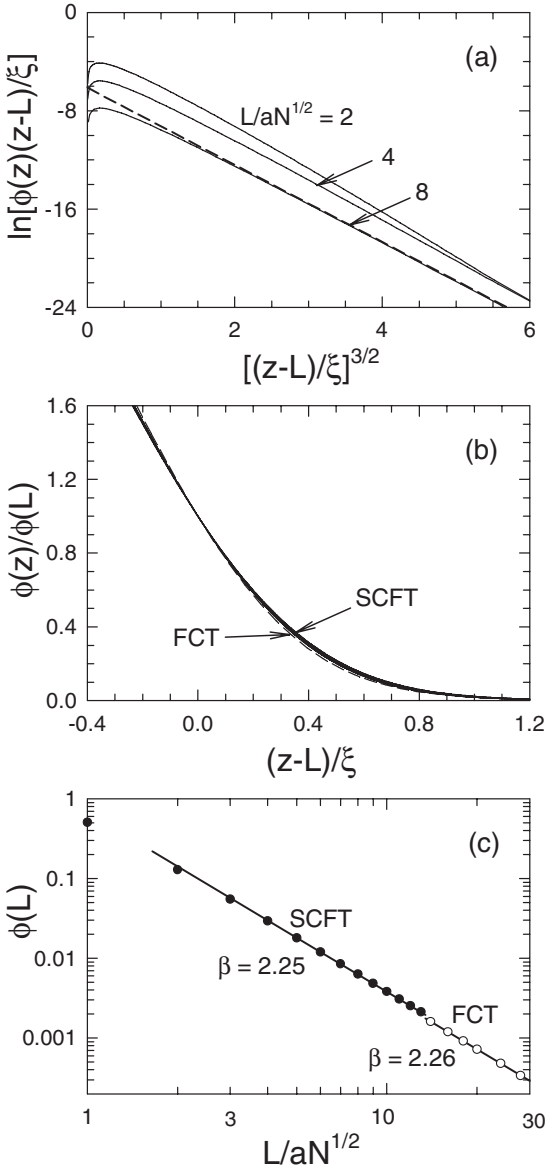

Fig. 5. Analogous plots to those in Figure 4, but for the overall concentration. In this case, (a) tests equation (49), (b) collapses the profiles in Figure 1b, and (c) demonstrates the power law behavior, $\phi(L) \sim L^{-\beta}$.

z_0/ξ, the SCFT curves for $L/aN^{1/2} = 2$, 4 and 8 in Figure 1a collapse onto a single master curve for $z_0 > L$. The same happens for the FCT, but thicker brushes (*e.g.*, $L/aN^{1/2} \sim 10$) are required and the master curve is slightly different.

Naturally, the amplitude of the tail, $g(L)$, should vanish as L diverges. Figure 4c suggests that this happens according to the power law,

$$g(L) \sim L^{-\alpha}\,, \tag{48}$$

with an exponent of $\alpha \approx 1.58$. Our SCFT calculations can only access brushes up to $L/aN^{1/2} \approx 13$, but we can go somewhat further with the FCT. A fit to the FCT at larger L gives a slightly bigger exponent of $\alpha \approx 1.61$, which suggests that the true exponent for the thick-brush limit is still a bit larger.

Continuing with the classical Milner-Witten approach [13], we now examine the concentration profile, $\phi(z)$. Because the field for $z > L$ is assumed to be zero, the fN segments of a chain extending outside the brush are distributed uniformly from $z = L$ to $z = z_0$. The integral of this concentration over $g(z_0)$ from equation (46) then results in an incomplete gamma function, which can

be approximated to give

$$\phi(z) \approx \frac{4kg(L)\xi}{3\pi^2(z-L)}\sqrt{\frac{\xi}{L}}\exp\left(-\pi\left(\frac{z-L}{\xi}\right)^{3/2}\right). \quad (49)$$

As confirmed in Figure 5a, the SCFT results conform to this expression (again with $k = 1.34$) even though the derivation ignores fluctuations about the classical path. Again, the analytical expression is not valid for the initial part of the tail, $L < z \lesssim L + \xi$.

Nevertheless the entire tail, $z > L$, of the concentration profile does exhibit a universal shape as illustrated in Figure 5b by the fact that the SCFT curves in Figure 1b collapse to a single curve when $\phi(z)$ and z are normalized by $\phi(L)$ and ξ, respectively. Again a nearly identical master curve results from the FCT calculation.

The behavior of $\phi(L)$ can be deduced by considering the total number of segments in the tail. On the one hand, it is given by the integral of $fNg(z_0)$ over $z_0 > L$, which must scale as $\sim g(L)\xi^{3/2}L^{-1/2}$ according to Figure 4b. On the other hand, it is also equal to the integral of $\phi(z)$ over $z > L$, which goes as $\sim \phi(L)\xi$ according to Figure 5b. The equivalence implies that

$$\phi(L) \sim L^{-\beta}, \quad (50)$$

with an exponent given by

$$\beta = \alpha + 2/3. \quad (51)$$

Figure 5c illustrates the power law decay of $\phi(L)$ and extracts an exponent, $\beta \approx 2.25$, in good agreement with equation (51).

3.3 Free energy

Previous studies have paid little attention to the free energy of the brush, presumably because $g(z_0)$ and $\phi(z)$ are the quantities most accessible to experiment and simulation. Nevertheless, the free energy is important because it relates to the force required to deform the brush [3], by, for example, compressing it, applying a lateral shear, or inserting a particle [25]. For brushes where the chains adsorb to the substrate as opposed to being covalently bonded, the free energy dictates the equilibrium value of σ [9]. Free energy is also the quantity that controls the level of composition fluctuations in $\hat{\phi}(\mathbf{r})$ [26]. For us, examination of the free energy provides one more way of validating our finite-stretching corrections.

To a first approximation, the SCFT free energy is given by $F \approx F_0 + nk_BT\ln(2/\sqrt{3})$, where F_0 is the SST prediction in equation (27) and the logarithmic term accounts for the proportionality factor in equation (10). The next most important contribution originates from the depletion layer, for which there are two parts. First there is the increased stretching energy, ΔF_e, which is estimated by averaging $\Delta f_e(z_0)$ in equation (39) over the classical $g_0(z_0)$ distribution in equation (26). Because of the way the depletion layer scales with L (see Fig. 3), we obtain the simple expression,

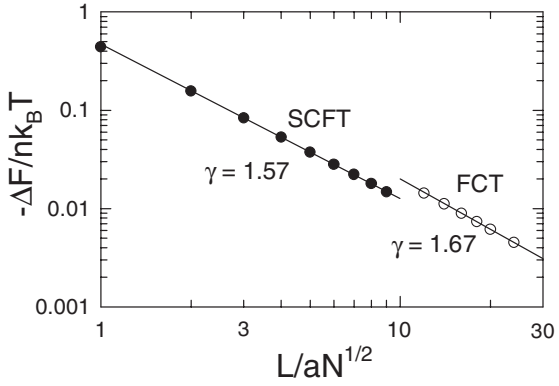

Fig. 6. Residual free energy, $\Delta F \equiv F - F_0 - nk_BT\ln(2/\sqrt{3}) - \Delta F_e - \Delta F_u$, remaining after the SST is corrected for the depletion layer. Analogous results are also shown for the FCT (open circles), for which $\Delta F \equiv F - F_0$.

$$\frac{\Delta F_e}{nk_BT} = \ln\left(\frac{\mu}{\epsilon}\right) - 0.1532. \quad (52)$$

Second, there is the change in the interaction energy from equation (40), which reduces to a simple constant,

$$\frac{\Delta F_u}{nk_BT} \approx \frac{\Lambda}{2aN^{1/2}}\int_0^\infty [\phi(z) - \phi_0(0)]^2\,\mathrm{d}z = 0.2854, \quad (53)$$

on account of the scaling. With these two contributions, the SCFT free energy can now be expressed as

$$\frac{F}{nk_BT} = \frac{9\pi^2}{40}\left(\frac{L}{aN^{1/2}}\right)^2 - 0.9852 - \ln\left(\frac{L^2\epsilon}{a^3N^{3/2}}\right) + \frac{\Delta F}{nk_BT}, \quad (54)$$

where ΔF represents the remaining corrections.

Figure 6 demonstrates that the residual energy can be fit to the power law,

$$\Delta F \sim -L^{-\gamma}. \quad (55)$$

Numerical inaccuracies in our SCFT calculations prevent us from considering ΔF at $L/aN^{1/2} \gtrsim 10$, but again the FCT calculations are capable of going somewhat further. Of course, the depletion layer is absent from the FCT, and so in that case the residual free energy is just $\Delta F = F - F_0$. The fact that FCT produces a consistent exponent implies that the main effect of the depletion layer has been properly removed from our SCFT expression for ΔF. The FCT exponent, $\gamma \approx 1.67$, is somewhat larger than the SCFT one, $\gamma \approx 1.57$, primarily because the fit has been done at larger L; naturally this implies that the true exponent for the thick-brush limit is even larger.

4 Discussion

Although the depletion layer at the grafting surface has been well documented by past numerical SCFT calculations [6–8], simulations [10–12] and experiment [9], there

has been relatively little attention paid to its width, μ, or concentration profile, $\phi(z)$. The cause is certainly clear; an entropic repulsion is created because the impenetrable substrate impedes chain fluctuations about the classical paths, which incidentally explains why the effect is absent from the classical theories. It is basically the same mechanism that creates the depletion layer in polymer solutions next to solid walls [27], but, of course, the details are different when the polymers are not attached. This fact was appreciated as early as 1980 when de Gennes [16] predicted that the width should scale as $\mu \sim \sigma^{-1/2}$ with a concentration profile $\phi(z) \sim z^{2/3}$. However, his calculation was based on the early Alexander approach [5], and has never been reconsidered in terms of the newer theories. Recent studies [6,9,10] have investigated the location of the peak in $\phi(z)$, but this is not really a direct measure of μ; roughly speaking, the peak occurs when the increasing slope of the dashed curve in Figure 3 balances the decreasing slope of the parabolic profile in equation (24).

Even within mean-field theory, there will be additional effects that influence the details of the depletion layer. For instance, we have not included surface interactions, apart from the impenetrability and the covalent bonds anchoring the chain ends. Real substrates will generally have an affinity for either the polymer or the solvent. Although this affinity will break our scaling relations for the depletion layer, it is nevertheless easily incorporated in the theory of Section 2.4. The finite flexibility of real polymers may also be important, because like the substrate it impedes chain fluctuations. This could be investigated by substituting the Gaussian chain model by the wormlike chain model [28]. The finite spacing between grafting points could also have an appreciable effect on the depletion layer, in which case it might be important to fix the grafting points rather than allowing them to float freely within the grafting plane. This can certainly be done within SCFT, although it will break the translational symmetry that normally simplifies the calculation.

The tail region has received considerably more attention than the depletion layer. The first calculation by Witten *et al.* [14] predicted

$$g(z_0) \propto \exp\left(-\frac{2}{3}\left(\frac{z_0 - L}{\xi}\right)^{3/2}\right), \tag{56}$$

$$\phi(z) \propto \exp\left(-\frac{4}{3}\left(\frac{z - L}{\xi}\right)^{3/2}\right), \tag{57}$$

using assumptions based on the ground-state-dominance approximation [18]. The calculation was performed for opposing dry brushes, but it is thought that the results equally apply to semi-dilute brushes [8,15]. A couple of years later, Milner and Witten [13] calculated similar expressions based on a FCT approach, but they found that the coefficients in the exponentials were both $-\pi$ instead of $-2/3$ and $-4/3$. They confirmed their prediction for $g(z_0)$ with a numerical SCFT calculation, but they did not examine the tail of $\phi(z)$. References [8] and [15] have since demonstrated that $\ln \phi(z)$ *versus* $[(z-L)/\xi]^{3/2}$ is linear at large z, but neither reported the resulting coefficient (*i.e.*, slope). Figures 4a and 5a now provide conclusive evidence that the coefficients for $g(z_0)$ and $\phi(z)$ are both $-\pi$. Furthermore, they also confirm that the predicted amplitudes of $g(z_0)$ and $\phi(z)$ in equations (46) and (49) are indeed related by a common factor of $k \approx 1.34$.

In another study, Netz and Schick [7] found that the tail eventually exhibits the Gaussian form,

$$g(z_0) \propto \frac{z_0}{aN^{1/2}} \exp\left(-\frac{3z_0^2}{2a^2N}\right), \tag{58}$$

$$\phi(z) \propto \frac{aN^{1/2}}{z} \exp\left(-\frac{3z^2}{2a^2N}\right). \tag{59}$$

This does not actually contradict our results. Equations (46) and (49) are derived assuming that only a small fraction (*i.e.*, $f \ll 1$) of the chains stretches beyond the classical brush edge, which requires that $z_0 - L \ll L$. If we extended the horizontal axes of Figures 4a and 5a, the slope of our SCFT results would begin to deviate from $-\pi$ and follow curves given by equations (58) and (59). In fact, there is evidence of this already happening for $L/aN^{1/2} = 2$. For the larger $L/aN^{1/2}$ values, however, $g(z_0)$ and $\phi(z)$ would be so incredibly small by the time the Gaussian form took effect that their actual shape would be absolutely inconsequential.

The above discussions regarding the detailed shape of $g(z_0)$ and $\phi(z)$ only pertain to z_0 and z well beyond L. Figures 4b and 5b are the first to show that $g(z_0)/g(L)$ and $\phi(z)/\phi(L)$ converge to master curves for the entire tail beyond L when scaled with respect to ξ. Furthermore, Figures 4c and 5c are the first to illustrate that the amplitudes, $g(L)$ and $\phi(L)$, decay with L according to power laws, equations (48) and (50). This is not entirely surprising because similar scaling was reported previously for opposing dry brushes [20,21], although in that case there is no exponent β because $\phi(L) = 1/2$. Interestingly, the exponent for $g(L)$ in that system takes on a simple rational value of $\alpha = 1/3$ as justified by a numerical fit as well as a simple scaling argument [21]. We suspect that the true exponent for semi-dilute brushes is also rational, but the fact that $g(L)$ decays so quickly makes it difficult to extract numerically. Nevertheless, we can still predict a value based on a reasonable scaling argument, whereby we assume that the significant departure of $g(z_0)$ from equation (26) begins at $z_0 \approx L - \zeta$ eventually matching up with equation (46) at $z_0 \approx L + \xi$. From equation (26), it then follows that $g(L-\zeta) \sim \zeta^{1/2}L^{-3/2}$ and $g'(L-\zeta) \sim -g(L-\zeta)/\zeta$. Similarly, equation (46) predicts $g'(L+\xi) \sim -g(L+\xi)/\xi$. Assuming that ζ and ξ are relatively small, we expect both sets of expressions to correctly represent $g(L)$ and $g'(L)$. This requires $\zeta \sim \xi$, which means that ζ also scales as $\sim L^{-1/3}$. That, in turn, implies $g(L) \sim \xi^{1/2}L^{-3/2}$, which gives an exponent,

$$\alpha = 5/3, \tag{60}$$

in reasonable agreement with the fits in Figure 4c.

For dry brushes, the free-energy contribution from the tail, ΔF, scales with a rational exponent $\gamma = 2/3$ [17, 20,21], and so we might again expect a rational value for

semi-dilute brushes. If we simply assume that the chains in the tail each contributes an average energy of order k_BT, then it follows that $\Delta F \sim g(L)\xi$, which implies

$$\gamma = \alpha + 1/3\,. \tag{61}$$

This relation certainly holds for dry brushes, where $\alpha = 1/3$. However, if we take $\alpha = 5/3$ for semi-dilute brushes, then $\gamma = 2$ is significantly larger than the values indicated in Figure 6. Perhaps we have overlooked an important contribution to the free energy, or maybe the depletion layer is not properly accounted for by equations (52) and (53). However, the fact that the FCT produces a consistent exponent to SCFT suggests otherwise. We believe that the true value of γ simply does not emerge until L is extremely large. If we consider the principal contribution to ΔF, which comes from $\int g \ln g \mathrm{d}z_0$, Figure 4b implies that the tail portion of the integral scales as $\sim g(L)\xi$ once the L-dependence of $\ln g(L)$ becomes sufficiently weak, and indeed this requires a very large L. It is impractical to test our suspicions by pushing the numerical FCT calculation to higher L, but the problem might be resolved with an analytical treatment along the lines of that in reference [17] for dry brushes.

5 Conclusions

We have examined the scaling behavior of the two dominant corrections to the classical strong-stretching theory (SST) for semi-dilute brushes in good solvent. The first correction originates from the impenetrability of the grafting surface, which causes a depletion of segments next to the substrate. By adapting a theory of Likhtman and Semenov [17], we predict a universal shape for the concentration profile, $\phi(z)$, of the depletion layer with a width that scales as $\mu \sim L^{-1}$. The prediction is confirmed by quantitative comparisons to self-consistent field theory (SCFT). The second correction involves a tail that extends beyond the classical brush height, L, primarily due to the translational entropy of the end-segment distribution, $g(z_0)$, as evident from the fact that it is well accounted for by the full classical theory (FCT). We demonstrate that the tails of $g(z_0)$ and $\phi(z)$ have universal shapes with a range that scales as $\xi \sim L^{-1/3}$ and amplitudes that decay as $g(L) \sim L^{-5/3}$ and $\phi(L) \sim L^{-7/3}$. We also calculate analytical expressions (46) and (49) for $g(z_0)$ and $\phi(z)$, respectively, at the extremity of the tail using the classical approach of Milner and Witten [13]. Furthermore, we derive an expression (54) for the free energy that improves vastly upon the simple SST prediction. Not only do these finite-stretching corrections provide valuable insights into the behavior of semi-dilute brushes, they also remain reasonably accurate down to experimentally relevant thicknesses of $L/aN^{1/2} \sim 2$.

This work was supported by EPSRC (EP/D031494/1).

References

1. S.T. Milner, Science **251**, 905 (1991).
2. S.F. Edwards, Proc. Phys. Soc. London **85**, 613 (1965).
3. S.T. Milner, T.A. Witten, M.E. Cates, Macromolecules **21**, 2610 (1988).
4. A.N. Semenov, Sov. Phys. JETP **61**, 733 (1985).
5. S. Alexander, J. Phys. (Paris) **38**, 983 (1977).
6. R. Baranowski, M.D. Whitmore, J. Chem. Phys. **103**, 2343 (1995).
7. R.R. Netz, M. Schick, Macromolecules **31**, 5105 (1998).
8. S.T. Milner, J. Chem. Soc. Faraday Trans. **86**, 1349 (1990).
9. M.S. Kent, L.T. Lee, B.J. Factor, F. Rondelez, G.S. Smith, J. Chem. Phys. **103**, 2320 (1995).
10. M.P. Pépin, M.D. Whitmore, J. Chem. Phys. **111**, 10381 (1999).
11. C. Seidel, R.R. Netz, Macromolecules **33**, 634 (2000).
12. T. Kreer, S. Metzger, M. Müller, K. Binder, J. Chem. Phys. **120**, 4012 (2004).
13. S.T. Milner, T.A. Witten, Macromolecules **25**, 5495 (1992).
14. T.A. Witten, L. Leibler, P.A. Pincus, Macromolecules **23**, 824 (1990).
15. H. Orland, M. Schick, Macromolecules **29**, 713 (1996).
16. P.G. de Gennes, Macromolecules **13**, 1069 (1980).
17. A.E. Likhtman, A.N. Semenov, Europhys. Lett. **51**, 307 (2000).
18. P.G. de Gennes, *Scaling Concepts in Polymer Physics* (Cornell University Press, Ithaca, 1979).
19. M.W. Matsen, in *Soft Matter*, Vol. **1**: *Polymer Melts and Mixtures*, edited by G. Gompper, M. Schick (Wiley-VCH, Weinheim, 2006).
20. M.W. Matsen, J. Chem. Phys. **121**, 1938 (2004).
21. M.W. Matsen, J. Chem. Phys. **117**, 2351 (2002).
22. R.R. Netz, M. Schick, Europhys. Lett. **38**, 37 (1997).
23. M.W. Matsen, J.M. Gardiner, J. Chem. Phys. **118**, 3775 (2003).
24. When comparing our results with those of reference [7], be aware that they measure distances in terms of $\hat{z} \equiv (\pi^2/6)^{1/3}L$ and they characterize the brush by the parameter $\beta \equiv (3\pi^4/32)^{1/3}L^2/a^2N$.
25. J.U. Kim, B. O'Shaughnessy, Phys. Rev. Lett. **89**, 238301 (2002); Macromolecules **39**, 413 (2006).
26. G.E. Yakubov, B. Loppinet, H. Zhang, J. Rühe, R. Sigel, G. Fytas, Phys. Rev. Lett. **92**, 115501 (2004).
27. D. Ausserré, H. Hervet, F. Rondelez, Phys. Rev. Lett. **54**, 1948 (1985).
28. K. Takahashi, Y. Yunoki, J. Phys. Soc. Jpn. **22**, 219 (1967); D.C. Morse, G.H. Fredrickson, Phys. Rev. Lett. **73**, 3235 (1994).